Journal of Atmospheric Chemistry **8** (1989) 41–62.

Ultraviolet Absorption Spectrum of Trifluoro-Bromo-Methane, Difluoro-Dibromo-Methane and Difluoro-Bromo-Chloro-Methane in the Vapor Phase

D. GILLOTAY and P. C. SIMON
Institut d'Aéronomie Spatiale de Belgique, Avenue Circulaire, 3, B-1180 Brussels, Belgium

(Received: 25 July 1988; in revised form: 5 December 1988)

Abstract. Ultraviolet absorption cross-sections of trifluoro-bromo-methane (CF_3Br-Halon 1301), difluoro-dibromo-methane (CF_2Br_2-Halon 1202) and of difluoro-bromo-chloro-methane (CF_2BrCl-Halon 1211) are measured in the wavelength interval 172–304 nm for temperatures ranging from 210 to 295 K with uncertainties of between 2 and 4%. They are compared with previous measurements available at room temperature. Temperature effects are discussed and parametrical formulae are proposed to compute the absorption cross-sections for wavelengths and temperatures useful in atmospheric modelling calculations. Photodissociation coefficients are presented and their temperature dependence is discussed.

Key words. Bromo-fluoro-methanes, UV absorption cross-sections, photodissociation coefficients, temperature dependence.

1. Introduction

Recent studies (Prather *et al.*, 1984; Rodriguez *et al.*, 1986; Yung *et al.*, 1980) have shown that brominated compounds can play a significant role in the catalytic destruction of ozone in the stratosphere.

RBr concentrations have been measured in the atmosphere by several authors (Fabian *et al.*, 1981; Lal *et al.*, 1985; Cicerone *et al.*, 1988; Berg *et al.*, 1984; Penkett *et al.*, 1985; Class *et al.*, 1986), confirming their possible impact on the ozone layer. The values of the ozone depletion efficiency relative to CFC-11 are estimated at the present time to be included between 10 and 11.4 for Halon 1301 and between 2.7 and 3.0 for the Halon 1211 (Brasseur and Simon, 1988).

The reliability of models is strongly dependent on the photodissociation pattern adopted for these bromocarbons. Until now, only one set of measurements of absorption cross-sections has been available for most of the bromocarbons at room temperature (Molina *et al.*, 1982).

The purpose of this paper is to report a new investigation of ultraviolet absorption cross-sections of three brominated methanes (CF_3Br, CF_2Br_2 and CF_2BrCl) measured between 172 and 300 nm, for temperatures between 295 and

210 K. The temperature dependence of the absorption cross-section is clearly demonstrated. Photodissociation coefficients are calculated and their temperature dependence is discussed.

2. Experimental

The absorption measurements have been performed by means of a single beam experimental device previously described (Gillotay and Simon, 1988) including a deuterium or a tungsten filament light source, a 1 m McPherson 225 monochromator, a 2 m thermostat absorption cell and a EMR type 542 P-09-18 solar blind photomultiplier. The temperature is regulated down to 210 K by circulation of cooled methylcyclohexane through a double jacket around the absorption cell and is determined with a precision better than 1% at 210 K. The pressure ranging from 2×10^{-3} to 1000 torr are measured with three capacitance manometers (MKS-Baratron) with a precision better than 0.1%.

Determination of absorption cross-sections is made after at least 15 sequential recordings of the incident and absorbed fluxes measured for identical temperature conditions, using Beer–Lambert's law.

The three 'Halon' provided by Kali Chemie were of an analytical grade and used after vacuum distillation and thorough outgassing. The gas phase chromatography does not reveal any impurities of a concentration greater than 0.1%.

3. Results

Numerical values of absorption cross-sections for selected wavelengths between 168 and 304 nm (2 nm intervals) and wavenumber intervals of 500 cm^{-1} currently used for aeronomy modeling (Brasseur and Simon, 1981) are respectively given in Tables IIa–IVa and IIb–IVb.

The absorption spectra are illustrated in Figures 1–6.

3.1. *Ambient Temperature* (295 K)

At ambient temperature, the measurements have been performed at working pressures given in Table I. In all cases, the Beer–Lambert law was found to hold for absorptions ranging from 10 to 85%.

Table I. Pressure ranges used for the absorption cross-section measurements

Compound	Pressure (torr)		
	295 K	255 K	210 K
CF_3Br	$722\text{–}6 \times 10^{-1}$	$597\text{–}6 \times 10^{-1}$	$384.6\text{–}2 \times 10^{-2}$
CF_2Br_2	$234\text{–}3 \times 10^{-2}$	$67\text{–}1 \times 10^{-1}$	$3.4\text{–}2 \times 10^{-2}$
CF_2BrCl	$453\text{–}1 \times 10^{-1}$	$80\text{–}8 \times 10^{-2}$	$10.3\text{–}9 \times 10^{-2}$

In such conditions and according to the error budget recently published by Simon *et al.* (1988), the absorption cross-sections given in Tables II–IV are determined to within an accuracy of ±2%.

Table IIa. Absorption cross-sections of CF_3Br at 2 nm intervals for five selected temperatures (295, 270, 250, 230, and 210 K)

λ(nm)	$\sigma(\lambda) \times 10^{21}$ (cm^2 molec^{-1})				
	295 K	270 K	250 K	230 K	210 K
168	5.17	5.09	5.04	4.98	4.93
170	6.96	6.89	6.84	6.79	6.73
172	9.28	9.24	9.21	9.17	9.14
174	12.2	12.3	12.3	12.3	12.3
176	16.0	16.1	16.2	16.3	16.4
178	20.5	20.8	21.1	21.3	21.6
180	26.1	26.6	27.1	27.5	28.0
182	32.6	33.5	34.3	35.0	35.8
184	40.2	41.6	42.7	43.9	45.1
186	48.8	50.8	52.4	54.1	55.9
188	58.2	60.9	63.2	65.5	67.9
190	68.4	71.9	74.8	77.8	81.0
192	78.8	83.2	86.9	90.7	94.7
194	89.3	94.6	99.0	104	108
196	99.4	105	110	116	121
198	109	115	121	127	133
200	116	123	129	136	142
202	122	130	136	142	149
204	126	133	139	146	152
206	128	134	140	146	152
208	127	132	137	142	148
210	123	128	132	136	140
212	117	121	124	127	130
214	110	112	114	116	118
216	101	102	102	103	104
218	90.6	90.3	90.1	89.9	89.7
220	79.9	78.6	77.6	76.6	75.6
222	69.2	67.1	65.4	63.8	62.3
224	58.8	56.1	54.1	52.1	50.1
226	49.1	46.1	43.8	41.6	39.5
228	40.3	37.1	34.7	32.5	30.5
230	32.4	29.3	27.0	25.0	23.0
232	25.7	22.8	20.7	18.8	17.1
234	20.0	17.4	15.6	13.9	12.4
236	15.3	13.1	11.5	10.1	8.88
238	11.6	9.66	8.35	7.22	6.24
240	8.62	7.04	5.98	5.09	4.33
242	6.33	5.06	4.23	3.54	2.96
244	4.59	3.59	2.95	2.43	2.00
246	3.28	2.52	2.04	1.65	1.33
248	2.32	1.75	1.39	1.11	0.881
250	1.63	1.20	0.941	0.738	0.579
252	1.13	0.818	0.632	0.489	0.378

Table IIa (*continued*)

λ(nm)	$\sigma(\lambda) \times 10^{21}$ (cm^2 molec^{-1})				
	295 K	270 K	250 K	230 K	210 K
254	0.777	0.554	0.422	0.322	0.246
256	0.530	0.373	0.281	0.212	0.160
258	0.360	0.250	0.186	0.139	0.104
260	0.243	0.167	0.123	0.0911	0.0674
262	0.164	0.111	0.0817	0.0600	0.0440
264	0.110	0.0742	0.0542	0.0396	0.0290
266	0.0736	0.0496	0.0362	0.0264	0.0192
268	0.0494	0.0333	0.0243	0.0177	0.0129
270	0.0331	0.0225	0.0164	0.0120	0.00882
272	0.0223	0.0153	0.0112	0.00829	0.00611
274	0.0151	0.0105	0.00779	0.00580	0.00432
276	0.0103	0.00725	0.00547	0.00414	0.00313
278	0.00706	0.00509	0.00392	0.00301	0.00232
280	0.00489	0.00363	0.00286	0.00225	0.00177

Table IIb. Absorption cross-sections of CF_3Br averaged over the spectral intervals used in atmospheric modeling calculations for five selected temperatures (295, 270, 250, 230, and 210 K) (wavenumber intervals: 500 cm^{-1})

No.	$\sigma(\lambda) \times 10^{21}$ (cm^2 molec^{-1})					
	λ(nm)	295 K	270 K	250 K	230 K	210 K
43	169.5–172.4	7.99	7.93	7.88	7.84	7.79
44	172.4–173.9	10.9	10.9	10.9	10.9	10.9
45	173.9–175.4	13.4	13.4	13.4	13.5	13.5
46	175.4–177.0	16.4	16.5	16.6	16.7	16.8
47	177.0–178.6	20.0	20.3	20.5	20.8	21.0
48	178.6–180.2	24.3	24.8	25.2	25.5	25.9
49	180.2–181.8	29.2	29.9	30.5	31.1	31.7
50	181.8–183.5	35.0	36.0	36.9	37.8	38.7
51	183.5–185.2	41.6	43.1	44.4	45.6	46.9
52	185.2–186.9	49.0	51.0	52.7	54.4	56.2
53	186.9–188.7	57.3	59.9	62.1	64.3	66.7
54	188.7–190.5	65.8	69.1	71.8	74.7	77.7
55	190.5–192.3	75.7	79.8	83.2	86.8	90.6
56	192.3–194.2	85.4	90.3	94.5	98.8	103
57	194.2–196.1	95.2	101	106	111	116
58	196.1–198.0	104	111	116	122	128
59	198.0–200.0	113	120	125	132	138
60	200.0–202.0	120	127	133	139	146
61	202.0–204.1	125	132	138	144	151
62	204.1–206.2	127	134	140	146	152
63	206.2–208.3	127	133	139	144	150
64	208.3–210.5	124	130	134	138	143
65	210.5–212.8	119	122	125	129	132
66	212.8–215.0	110	113	114	116	118
67	215.0–217.4	99.7	101	101	102	103

Table IIb (*continued*)

No.	$\sigma(\lambda) \times 10^{21}$ (cm^2 molec^{-1})					
	λ(nm)	295 K	270 K	250 K	230 K	210 K
68	217.4–219.8	87.4	86.8	86.4	85.9	85.4
69	219.8–222.2	74.6	72.8	71.5	70.1	68.8
70	222.2–224.7	61.6	59.1	57.1	55.2	53.3
71	224.7–227.3	49.1	46.1	43.8	41.6	39.5
72	227.3–229.9	37.8	34.6	32.3	30.1	28.1
73	229.9–232.6	28.1	25.4	22.9	20.9	19.1
74	232.6–235.3	20.1	17.5	15.7	14.0	12.5
75	235.3–238.1	13.9	11.8	10.3	8.99	7.86
76	238.1–241.0	9.29	7.63	6.51	5.56	4.75
77	241.0–243.9	5.89	4.69	3.90	3.25	2.71
78	243.9–246.9	3.63	2.80	2.28	1.85	1.51
79	246.9–250.0	2.13	1.59	1.26	1.00	0.794
80	250.0–253.2	1.24	0.901	0.699	0.542	0.421
81	253.2–256.4	0.667	0.473	0.359	0.272	0.207
82	256.4–259.7	0.360	0.250	0.186	0.139	0.104
83	259.7–263.2	0.181	0.123	0.0905	0.0666	0.0490
84	263.2–266.7	0.0899	0.0607	0.0443	0.0323	0.0236
85	266.7–270.3	0.0447	0.0301	0.0220	0.0161	0.0117
86	270.3–274.0	0.0219	0.0150	0.0110	0.00814	0.00600
87	274.0–277.8	0.0105	0.00738	0.00557	0.00421	0.00317
88	277.8–281.7	0.00507	0.00375	0.00294	0.00231	0.00182

Table IIIa. Absorption cross-sections of CF_2Br_2 at 2 nm intervals for five selected temperatures (295, 270, 250, 230, and 210 K)

λ(nm)	$\sigma(\lambda) \times 10^{21}$ (cm^2 molec^{-1})				
	295 K	270 K	250 K	230 K	210 K
170	1245	1108	1000	891	782
172	781	696	629	560	493
174	553	551	550	549	548
176	495	523	546	568	590
178	603	641	671	700	730
180	750	791	824	857	890
182	866	939	997	1056	1114
184	1009	1086	1148	1210	1272
186	1118	1204	1272	1341	1409
188	1180	1262	1327	1392	1458
190	1168	1252	1319	1387	1454
192	1109	1185	1245	1306	1366
194	1022	1085	1135	1185	1235
196	920	973	1016	1058	1100
198	825	869	905	941	976
200	748	792	827	862	898
202	716	758	791	825	858
204	735	778	812	846	880
206	810	853	887	921	955

Table IIIa (*continued*)

λ(nm)	$\sigma(\lambda) \times 10^{21}$ (cm^2 molec^{-1})				
	295 K	270 K	250 K	230 K	210 K
208	936	989	1033	1076	1119
210	1110	1173	1223	1273	1323
212	1431	1408	1466	1525	1583
214	1586	1670	1738	1806	1873
216	1841	1935	2011	2086	2162
218	2081	2186	2270	2353	2437
220	2281	2394	2482	2577	2676
222	2477	2585	2675	2767	2863
224	2540	2643	2729	2817	2909
226	2545	2640	2718	2800	2883
228	2493	2577	2646	2717	2790
230	2390	2461	2519	2578	2639
232	2246	2302	2347	2394	2442
234	2068	2109	2143	2177	2212
236	1869	1897	1918	1941	1964
238	1659	1674	1686	1698	1710
240	1448	1452	1455	1459	1463
242	1243	1238	1235	1232	1229
244	1050	1039	1031	1023	1015
246	875	860	848	836	825
248	718	701	687	674	661
250	582	564	549	535	521
252	466	447	433	419	406
254	369	351	337	325	312
256	289	272	260	248	237
258	224	209	198	189	178
260	172	159	150	141	132
262	130	119	112	104	97.3
264	98.7	89.6	82.9	76.7	71.0
266	74.0	66.5	61.0	56.0	51.3
268	55.1	48.9	44.5	40.5	36.8
270	40.8	35.9	32.3	29.1	26.3
272	30.1	26.1	23.3	20.8	18.6
274	22.1	18.9	16.7	14.8	13.1
276	16.1	13.7	12.0	10.5	9.17
278	11.7	9.81	8.51	7.38	6.39
280	8.52	7.04	6.04	5.18	4.44
282	6.17	5.03	4.27	3.62	3.08
284	4.47	3.59	3.02	2.53	2.13
286	3.23	2.56	2.13	1.77	1.47
288	2.34	1.83	1.50	1.23	1.01
290	1.69	1.30	1.06	0.856	0.695
292	1.22	0.928	0.744	0.596	0.478
294	0.876	0.663	0.525	0.415	0.329
296	0.645	0.474	0.370	0.290	0.226
298	0.470	0.340	0.262	0.202	0.156
300	0.343	0.244	0.186	0.142	0.108
302	0.252	0.176	0.132	0.0993	0.0746
304	0.185	0.127	0.0944	0.0699	0.0518

Table IIIb. Absorption cross-sections of CF_2Br_2 averaged over the spectral intervals used in atmospheric modeling calculations for five selected temperatures (295, 270, 250, 230, and 210 K) (wavenumber intervals: 500 cm^{-1})

No.	$\sigma(\lambda) \times 10^{21}$ (cm^2 $molec^{-1}$)					
	λ(nm)	295 K	270 K	250 K	230 K	210 K
43	169.5–172.4	1001	870	775	692	602
44	172.4–173.9	632	602	572	542	513
45	173.9–175.4	527	535	543	545	552
46	175.4–177.0	503	538	559	577	601
47	177.0–178.6	596	631	660	684	703
48	178.6–180.2	715	752	793	817	847
49	180.2–181.8	810	861	909	960	1001
50	181.8–183.5	912	993	1040	1105	1165
51	183.5–185.2	1025	1103	1180	1235	1300
52	185.2–186.9	1120	1209	1275	1343	1411
53	186.9–188.7	1170	1254	1324	1380	1454
54	188.7–190.5	1175	1253	1322	1389	1455
55	190.5–192.3	1115	1210	1270	1337	1385
56	192.3–194.2	1055	1130	1175	1215	1273
57	194.2–196.1	970	1015	1060	1100	1148
58	196.1–198.0	864	918	952	991	1035
59	198.0–200.0	780	827	861	898	922
60	200.0–202.0	721	768	801	838	872
61	202.0–204.1	712	768	803	836	869
62	204.1–206.2	766	824	842	873	915
63	206.2–208.3	882	932	968	999	1050
64	208.3–210.5	1054	1112	1157	1200	1250
65	210.5–212.8	1285	1354	1412	1476	1527
66	212.8–215.0	1562	1640	1714	1795	1850
67	215.0–217.4	1855	1952	2015	2096	2175
68	217.4–219.8	2144	2226	2305	2399	2486
69	219.8–222.2	2424	2533	2623	2717	2814
70	222.2–224.7	2529	2634	2721	2811	2904
71	224.7–227.3	2545	2640	2719	2800	2883
72	227.3–229.9	2467	2547	2613	2681	2750
73	229.9–232.6	2304	2366	2416	2468	2520
74	232.6–235.3	2073	2115	2149	2183	2218
75	235.3–238.1	1796	1819	1838	1857	1876
76	238.1–241.0	1500	1507	1512	1518	1524
77	241.0–243.9	1198	1192	1188	1183	1179
78	243.9–246.9	925	912	901	890	879
79	246.9–250.0	682	664	650	637	623
80	250.0–253.2	493	475	460	446	433
81	253.2–256.4	335	318	305	292	280
82	256.4–259.7	224	209	198	188	178
83	259.7–263.2	140	129	120	113	105
84	263.2–266.7	85.6	77.3	71.2	65.6	60.4
85	266.7–270.3	51.2	45.3	41.1	37.3	33.9
86	270.3–274.0	29.6	25.7	22.9	20.5	18.3
87	274.0–277.8	16.4	13.9	12.2	10.7	9.33
88	277.8–281.7	8.80	7.27	6.25	5.37	4.61
89	281.7–285.7	4.69	3.78	3.18	2.67	2.25

Table IIIb (*continued*)

No.	$\sigma(\lambda) \times 10^{21}$ (cm^2 molec^{-1})					
	λ(nm)	295 K	270 K	250 K	230 K	210 K
90	285.7–289.9	2.41	1.89	1.55	1.28	1.05
91	289.9–294.1	1.22	0.928	0.744	0.596	0.478
92	294.1–298.5	0.615	0.451	0.352	0.274	0.214
93	298.5–303.0	0.303	0.214	0.162	0.123	0.0930
94	303.0–307.7	0.131	0.0883	0.0644	0.0469	0.0342

Table IVa. Absorption cross-sections of CF_2BrCl at 2 nm intervals for five selected temperatures (295, 270, 250, 230, and 210 K)

λ(nm)	$\sigma(\lambda) \times 10^{21}$ (cm^2 molec^{-1})				
	295 K	270 K	250 K	230 K	210 K
170	3230	3200	3180	3160	3150
172	2342	2300	2285	2250	2227
174	1760	1720	1680	1660	1660
176	1209	1180	1175	1170	1145
178	847	840	834	830	825
180	581	580	579	579	578
182	419	419	418	418	418
184	350	353	356	359	362
186	341	347	353	359	366
188	389	405	420	437	456
190	474	500	524	548	573
192	584	626	666	707	748
194	722	768	816	866	922
196	845	919	974	1020	1078
198	990	1041	1090	1139	1190
200	1197	1244	1284	1324	1366
202	1230	1283	1328	1374	1422
204	1244	1302	1350	1400	1452
206	1239	1299	1350	1402	1457
208	1216	1277	1328	1381	1435
210	1177	1237	1286	1337	1391
212	1124	1180	1227	1276	1326
214	1060	1111	1154	1198	1245
216	986	1032	1070	1110	1151
218	907	947	980	1014	1049
220	824	858	885	914	943
222	741	768	790	813	836
224	659	680	697	714	732
226	580	595	608	620	633
228	505	516	524	533	541
230	436	442	447	452	457
232	373	376	378	380	382
234	316	316	316	316	316
236	266	264	262	260	259

Table IVa (*continued*)

λ(nm)	$\sigma(\lambda) \times 10^{21}$ (cm^2 molec^{-1})				
	295 K	270 K	250 K	230 K	210 K
238	222	218	215	212	210
240	183	179	175	172	168
242	150	145	141	138	134
244	123	117	113	109	106
246	99.2	94.0	90.0	86.1	82.5
248	79.7	74.7	70.9	67.3	63.9
250	63.7	59.0	55.5	52.2	49.1
252	50.5	46.2	43.1	40.2	37.5
254	39.8	36.0	33.3	30.7	28.3
256	31.2	27.9	25.5	23.3	21.3
258	24.3	21.4	19.4	17.5	15.9
260	18.8	16.4	14.7	13.1	11.7
262	14.5	12.4	11.0	9.73	8.61
264	11.1	9.39	8.21	7.18	6.28
266	8.46	7.05	6.09	5.26	4.54
268	6.42	5.26	4.49	3.83	3.26
270	4.84	3.90	3.29	2.77	2.33
272	3.63	2.88	2.39	1.99	1.65
274	2.71	2.11	1.73	1.42	1.16
276	2.01	1.54	1.24	1.00	0.810
278	1.48	1.11	0.887	0.706	0.562
280	1.09	0.803	0.629	0.493	0.386
282	0.796	0.576	0.444	0.342	0.264
284	0.579	0.410	0.311	0.236	0.179
286	0.419	0.290	0.216	0.161	0.120
288	0.301	0.204	0.149	0.109	0.0802
290	0.215	0.143	0.103	0.0737	0.0530
292	0.153	0.0990	0.0698	0.0493	0.0348
294	0.108	0.0683	0.0472	0.0327	0.0226
296	0.0761	0.0468	0.0317	0.0215	0.0146
298	0.0532	0.0318	0.0211	0.0140	0.00929
300	0.0369	0.0215	0.0139	0.00905	0.00587
302	0.0255	0.0144	0.00914	0.00579	0.00367

Table IVb. Absorption cross-sections of CF_2BrCl averaged over the spectral intervals used in atmospheric modeling calculations for five selected temperatures (295, 270, 250, 230, and 210 K) (wavenumber intervals: 500 cm^{-1})

No.	$\sigma(\lambda) \times 10^{21}$ (cm^2 molec^{-1})					
	λ(nm)	295 K	270 K	250 K	230 K	210 K
43	169.5–172.4	2770	2738	2710	2686	2661
44	172.4–173.9	1999	1960	1920	1880	1841
45	173.9–175.4	1575	1535	1498	1478	1449
46	175.4–177.0	1165	1147	1131	1115	1100
47	177.0–178.6	878	866	855	845	837

Table IVb (*continued*)

No.	$\sigma(\lambda) \times 10^{21}$ (cm^2 molec^{-1})					
	λ(nm)	295 K	270 K	250 K	230 K	210 K
48	178.6–180.2	643	642	641	641	641
49	180.2–181.8	487	487	487	487	487
50	181.8–183.5	388	390	391	391	392
51	183.5–185.2	341	347	352	357	361
52	185.2–186.9	342	350	356	362	367
53	186.9–188.7	384	399	415	430	444
54	188.7–190.5	448	472	492	515	538
55	190.5–192.3	550	587	620	653	703
56	192.3–194.2	665	717	760	805	852
57	194.2–196.1	799	840	893	947	1000
58	196.1–198.0	917	970	1030	1090	1150
59	198.0–200.0	1080	1131	1177	1223	1269
60	200.0–202.0	1196	1266	1309	1352	1397
61	202.0–204.1	1239	1296	1343	1391	1441
62	204.1–206.2	1243	1303	1353	1404	1458
63	206.2–208.3	1227	1288	1339	1391	1446
64	208.3–210.5	1191	1251	1300	1352	1406
65	210.5–212.8	1135	1191	1238	1288	1339
66	212.8–215.0	1063	1115	1158	1203	1249
67	215.0–217.4	979	1024	1062	1101	1141
68	217.4–219.8	882	920	951	984	1017
69	219.8–222.2	783	813	837	863	889
70	222.2–224.7	681	704	722	741	760
71	224.7–227.3	580	595	608	620	633
72	227.3–229.9	484	493	500	508	515
73	229.9–232.6	396	400	403	406	409
74	232.6–235.3	318	318	318	318	318
75	235.3–238.1	250	247	245	243	241
76	238.1–241.0	192	188	185	181	178
77	241.0–243.9	144	139	135	131	127
78	243.9–246.9	106	101	96.5	92.6	88.9
79	246.9–250.0	75.4	70.5	66.8	63.2	59.9
80	250.0–253.2	53.5	49.2	46.0	42.9	40.1
81	253.2–256.4	36.1	32.5	29.9	27.5	25.3
82	256.4–259.7	24.3	21.4	19.4	17.5	15.9
83	259.7–263.2	15.5	13.3	11.8	10.5	9.31
84	263.2–266.7	9.70	8.14	7.08	6.15	5.35
85	266.7–270.3	5.98	4.88	4.15	3.53	3.00
86	270.3–274.0	3.58	2.83	2.35	1.95	1.62
87	274.0–277.8	2.04	1.56	1.26	1.02	0.825
88	277.8–281.7	1.12	0.830	0.652	0.511	0.401
89	281.7–285.7	0.608	0.431	0.328	0.249	0.190
90	285.7–289.9	0.311	0.211	0.155	0.114	0.0835
91	289.9–294.1	0.153	0.0990	0.0698	0.0493	0.0348
92	294.1–298.5	0.0721	0.0442	0.0298	0.0202	0.0136
93	298.5–303.0	0.0318	0.0183	0.0118	0.00758	0.00487

The absorption cross-section measurements of CF_3Br, which have been extended down to 168 nm, are illustrated in Figure 1 and display a continuous absorption spectrum with a maximum close to 206 nm and cross-section values ranging from 1.3×10^{-19} cm^2 molec^{-1} at 206 nm to 6×10^{-24} cm^2 molec^{-1} at 280 nm. Comparison with the only available set of measurements published by Molina *et al.* (1982) show good agreement (within the experimental accuracy) between 190 and 225 nm and for wavelengths greater than 255 nm. Between 225 and 255 nm, the values proposed by Molina *et al.* (1982) are on average 15% lower than those reported here, except for one measurement at 240 nm where the difference reaches 34%.

CF_2Br_2 displays a continuous absorption spectrum with two maxima (respectively, at 188 and 225 nm) with cross-section values ranging from 2.5×10^{-18} cm^2 molec^{-1} to 1.8×10^{-22} cm^2 molec^{-1} at 304 nm (Figure 2). Comparison with the values previously published by Molina *et al.* (1982) show good agreement over the all spectral range except between 240 and 260 where the differences can reach a maximum of 10%.

For CF_2BrCl, as shown by Figure 3, a continuous absorption spectrum is also observed between 168 and 302 nm with a maximum at 204 nm and with cross-section values ranging from 1.2×10^{-18} cm^2 molec^{-1} at the maximum to 2.5×10^{-23} cm^2 molec^{-1} at 302 nm. In this case, the values proposed by Molina *et al.* (1982) are, on average, 20–25% lower than those reported here over the whole spectral range except for wavelengths greater than 295 nm.

The differences between the two sets of measurements are difficult to explain in terms of their accuracy. The purity of the compounds used in this work has been carefully checked (see Section 2). There is no indication of the level and nature of impurities in the products used by Molina *et al.* (1982).

3.2. *Low Temperature* (210–270 K)

Absorption cross-sections have been measured at three temperatures in the greatest range of pressure afforded by the vapor pressure conditions. The experimental conditions are summarized in Table I. The accuracy is ±3.5% according to the error budget published by Simon *et al.* (1988).

At low temperature, as can be seen on Figures 4–6, the absorption cross-sections show a temperature dependence depending on both the wavelength and the chemical composition of the compound. The absorption cross-sections decrease with temperature in the region of the longer wavelengths and increase in the region of the maximum of absorption. These effects are the most significant at the lower temperature.

For the three compounds, the analysis of the relationship of absorption cross-sections versus temperature for a given wavelength shows an exponential dependence on temperature in all the temperature and wavelength ranges con-

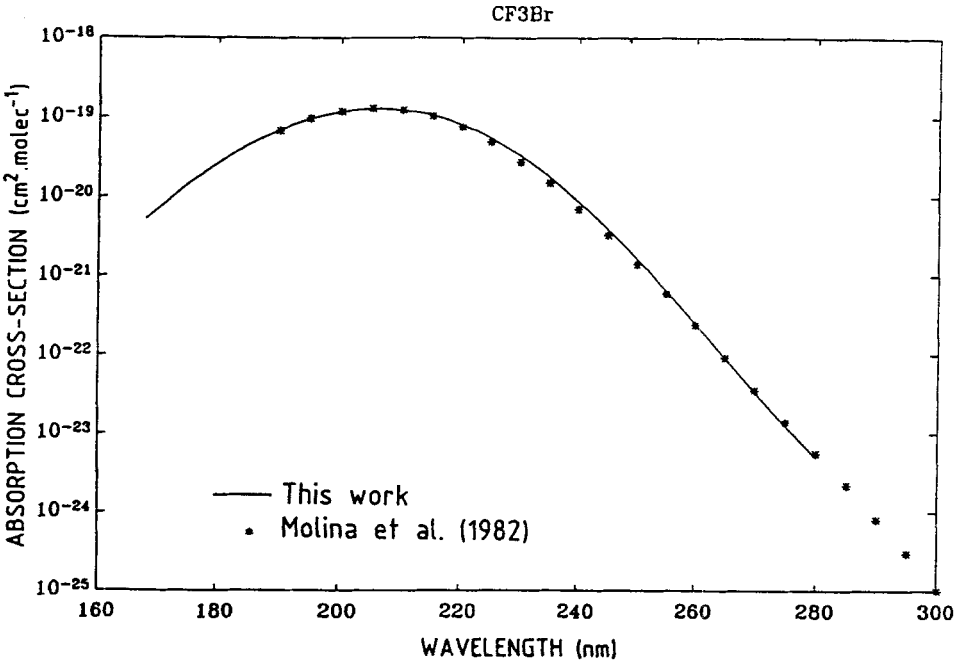

Fig. 1. Ultraviolet absorption cross-sections of CF_3Br at 295 K, between 170 and 300 nm.

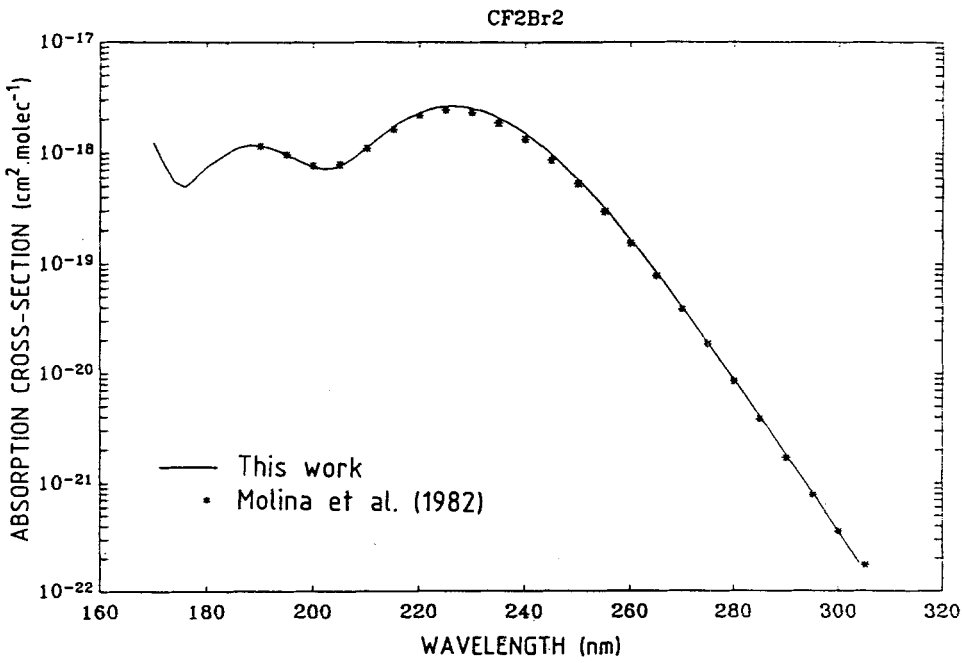

Fig. 2. Ultraviolet absorption cross-sections of CF_2Br_2 at 295 K, between 170 and 304 nm.

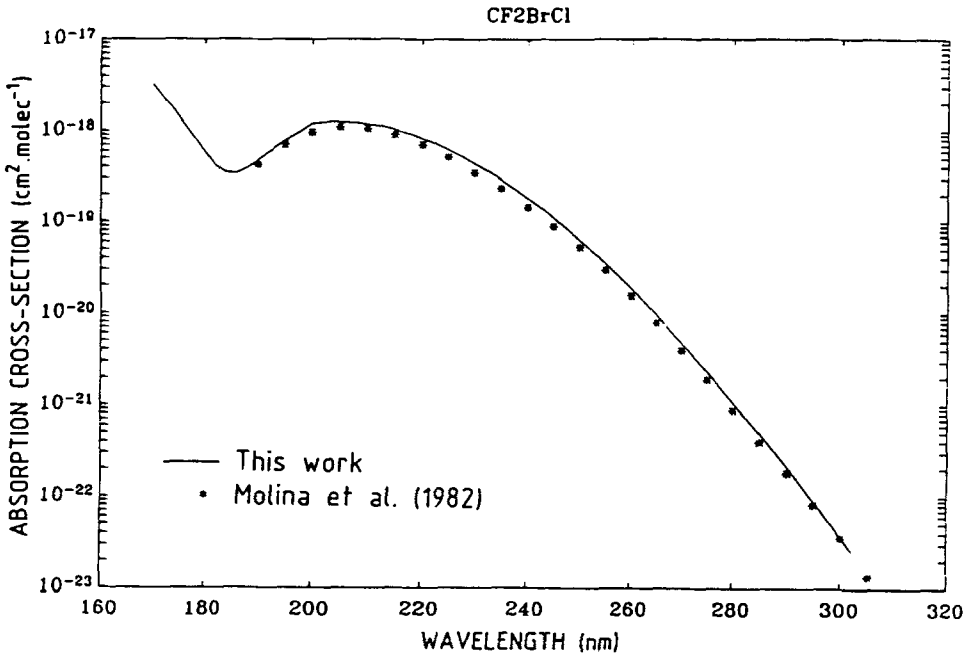

Fig. 3. Ultraviolet absorption cross-sections of CF_2BrCl at 295 K, between 170 and 302 nm.

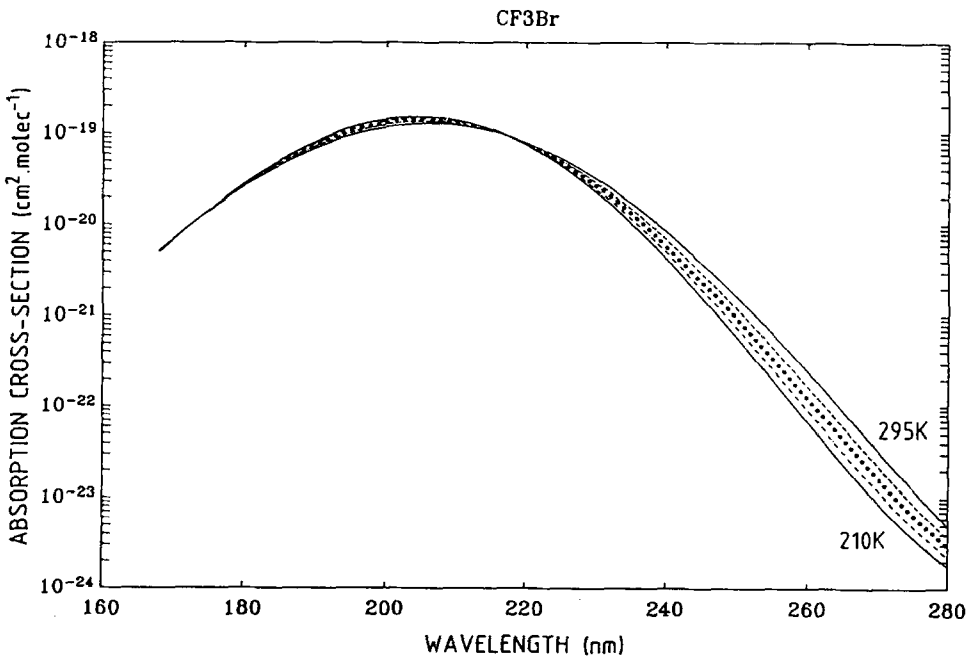

Fig. 4. Ultraviolet absorption cross-sections of CF_3Br versus wavelength as a function of temperature ($T = 295, 270, 250, 230, 210$ K).

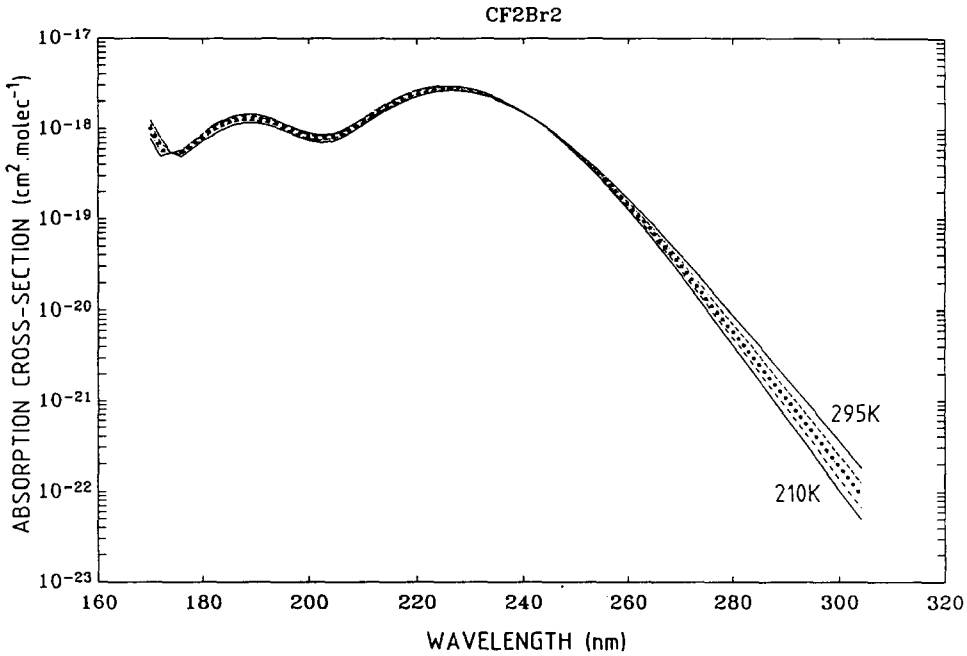

Fig. 5. Ultraviolet absorption cross-sections of CF_2Br_2 versus wavelength as a function of temperature ($T = 295, 270, 250, 230, 210$ K).

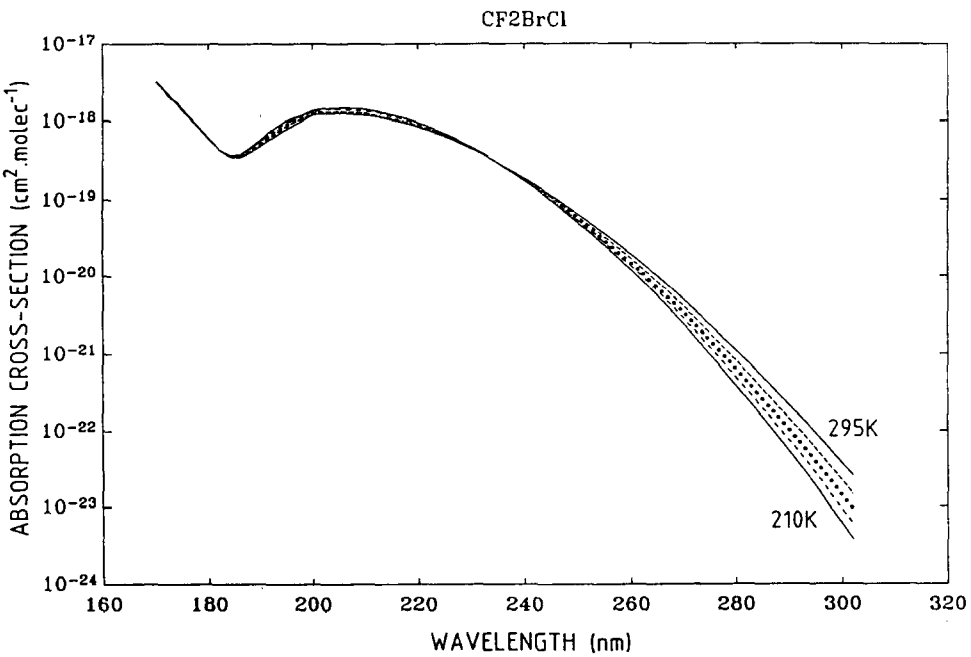

Fig. 6. Ultraviolet absorption cross-sections of CF_2BrCl versus wavelength as a function of temperature ($T = 295, 270, 250, 230, 210$ K).

sidered in this work. Figures 7–9 illustrate this exponential dependence for the longer wavelengths.

Numerical values deduced from a least-square fit through the three temperatures measured are presented in Tables II–IV for five defined temperatures (295, 270, 250, 230, 210 K) which cover the usual atmospheric temperature conditions.

As explained above, the absorption cross-sections can be represented by an empirical function of temperature for each wavelength according to the following expression

$$\log_{10}\sigma(\lambda) = A(\lambda) + B(\lambda) \times T, \tag{1}$$

where parameters A and B were determined by a polynomial least-square fit of the available experimental data with respect to temperature and wavelength to obtain the following polynomial expression

$$\log_{10}\sigma(\lambda, T) = A_0 + A_1\lambda + \cdots + A_n\lambda^n + (T-273) \times (B_0 + B_1\lambda + \cdots + B_n\lambda^n). \tag{2}$$

The computed values of A and B are given in Table V. The values of absorption cross-sections calculated with expression (2) represent all the experimental data with differences lower than ±4%.

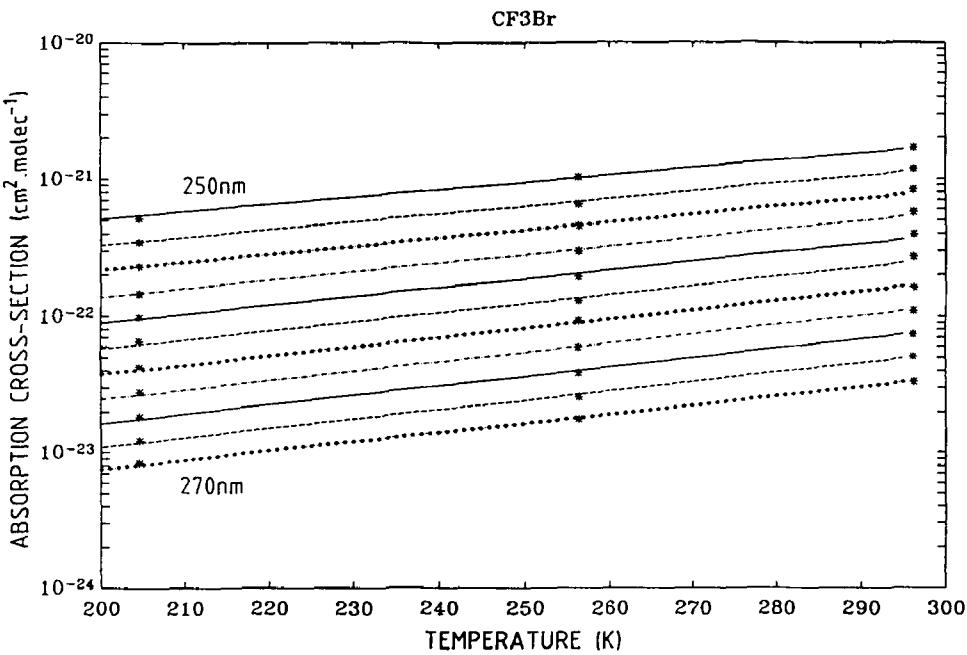

Fig. 7. Ultraviolet absorption cross-sections of CF_3Br, between 250 and 270 nm, versus temperature. Wavelength increment between successive curves is 2 nm.

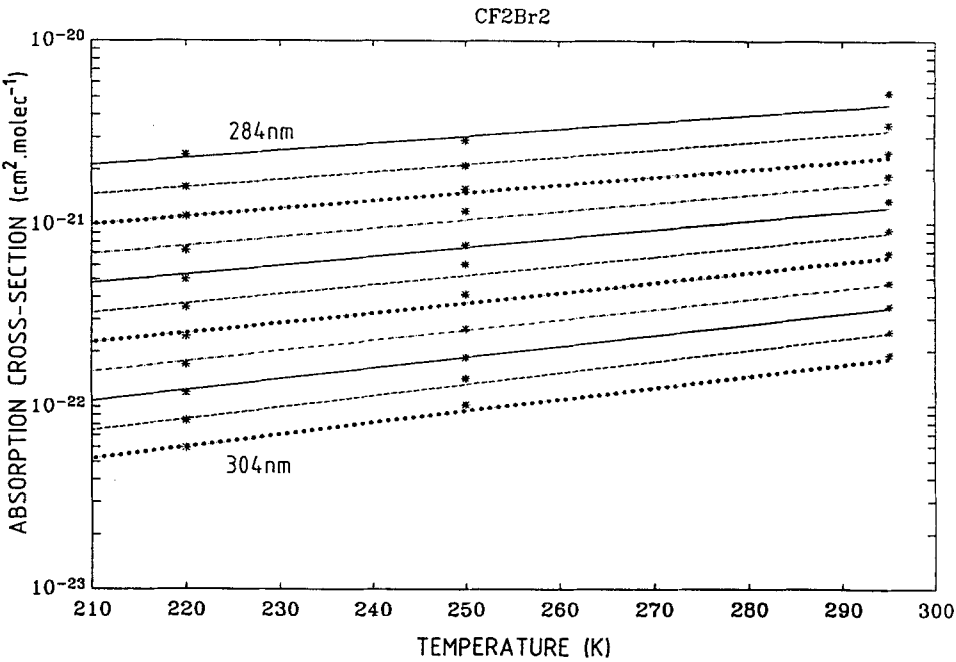

Fig. 8. Ultraviolet absorption cross-sections of CF_2Br_2, between 284 and 304 nm, versus temperature. Wavelength increment between successive curves is 2 nm.

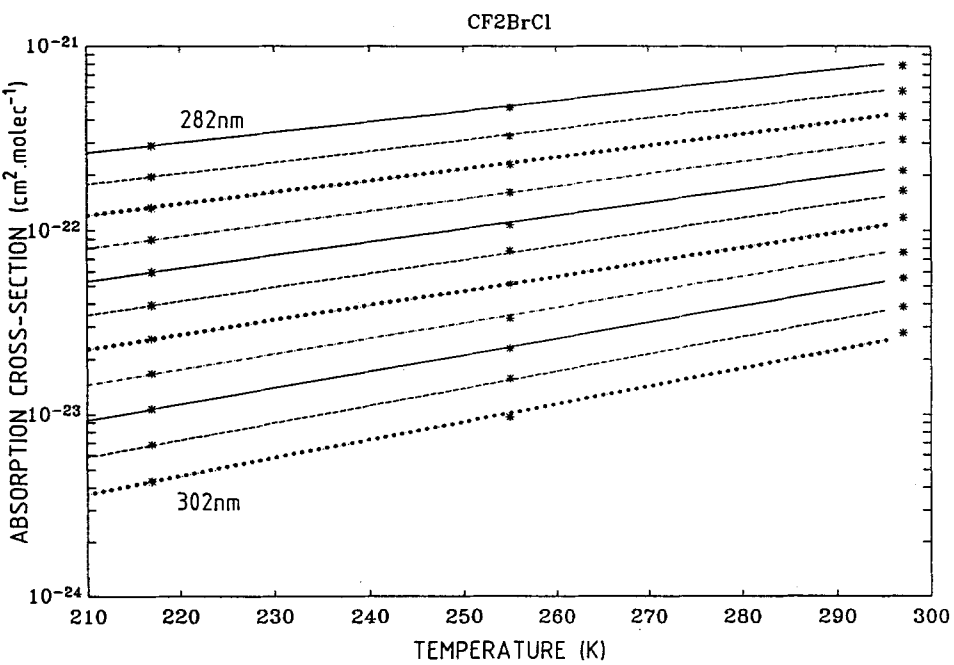

Fig. 9. Ultraviolet absorption cross-sections of CF_2BrCl, between 282 and 302 nm, versus temperature. Wavelength increment between successive curves is 2 nm.

Table V. Parameters A_i and B_i for polynomial expression of $\sigma(\lambda, T)$ of bromo-fluoro-methanes

CF_3Br	
$A_0 = 62.563$	$B_0 = -9.1755\ 10^{-1}$
$A_1 = -2.0068$	$B_1 = 1.8575\ 10^{-2}$
$A_2 = 1.6592\ 10^{-2}$	$B_2 = -1.3857\ 10^{-4}$
$A_3 = -5.6465\ 10^{-5}$	$B_3 = 4.5066\ 10^{-7}$
$A_4 = 6.7459\ 10^{-8}$	$B_4 = -5.3803\ 10^{-10}$
T range: 210–300 K	
λ range: 178–280 nm	
CF_2Br_2	
$A_0 = -206.28$	$B_0 = 1.0460\ 10^{-1}$
$A_1 = 2.3726$	$B_1 = -1.4124\ 10^{-3}$
$A_2 = -1.0527\ 10^{-2}$	$B_2 = 6.9015\ 10^{-6}$
$A_3 = 1.9239\ 10^{-5}$	$B_3 = -1.5164\ 10^{-8}$
$A_4 = -1.2242\ 10^{-8}$	$B_4 = 1.3990\ 10^{-11}$
T range: 210–300 K	
λ range: 222–304 nm	
CF_2BrCl	
$A_0 = -134.80$	$B_0 = 3.3070\ 10^{-1}$
$A_1 = 1.7084$	$B_1 = -5.0957\ 10^{-3}$
$A_2 = -9.1540\ 10^{-3}$	$B_2 = 2.9361\ 10^{-5}$
$A_3 = 2.1644\ 10^{-5}$	$B_3 = -7.6198\ 10^{-8}$
$A_4 = -1.9863\ 10^{-8}$	$B_4 = 7.6825\ 10^{-11}$
T range: 210–300 K	
λ range: 200–302 nm	

The relative values of absorption cross-sections $\sigma(T)/\sigma(295)$ versus wavelength relationships for a given temperature, display very similar features for all three compounds (Figures 10–12).

4. Discussion

Photodissociation coefficients J for a given altitude z, zenith angle x and wavelength interval have been computed according to the relations

$$J^z = \sigma_\lambda q_\lambda(z),$$

$$q_\lambda(z) = q_\lambda(\infty)\, e^{-\tau_\lambda(z)},$$

$$\tau_\lambda(z) = \int_z^\infty [n(O_2)\sigma(O_2) + n(O_3)\sigma(O_3) + n(\text{air})\sigma_{\text{scatt.}}] \sec\chi \, dz \qquad (3)$$

where σ is the absorption cross-section, $q_\lambda(z)$ and $q_\lambda(\infty)$ are the solar irradiance at altitude z or extraterrestrial ($z = \infty$), and n is the number of particles per volume unit, for solar zenith angles of 0° and 60° ($\sec\chi = 1$ and 2), taking the

values of $\sigma(O_2)$, $\sigma(O_3)$ from WMO (1985) and Kockarts (1976), of σ_{scatt} from Nicolet (1984) and the values of $q_\lambda(\infty)$ from WMO (1985), and taking into account the actual values of the cross-sections which correspond to the temperature conditions prevailing at a definite altitude.

A comparison of either temperature dependent or independent photodissociation coefficients for different stratospheric altitudes (15 to 50 km) is presented in Table VI, where relative photodissociation coefficients $J(T)/J(295)$ are given for the studied compounds. Obviously, the effect is maximum in the

Table VI. Photodissociation coefficients versus altitude in the stratosphere

Z(km)	sec $\chi = 1$			sec $\chi = 2$		
	$J(s^{-1})$ $\sigma(295\ K)^a$	$J(s^{-1})$ $\sigma = f(T)$	J_{rel}	$J(s^{-1})$ $\sigma(295\ K)^a$	$J(s^{-1})$ $\sigma = f(T)$	J_{rel}
CF_3Br (λ range 175–290 nm):						
15	$3.591\ 10^{-9}$	$4.115\ 10^{-9}$	1.146	$7.714\ 10^{-12}$	$8.957\ 10^{-12}$	1.161
20	$3.878\ 10^{-8}$	$4.447\ 10^{-8}$	1.147	$6.901\ 10^{-10}$	$8.004\ 10^{-10}$	1.160
25	$2.075\ 10^{-7}$	$2.351\ 10^{-7}$	1.133	$1.486\ 10^{-8}$	$1.704\ 10^{-8}$	1.147
30	$7.468\ 10^{-7}$	$8.296\ 10^{-7}$	1.111	$1.425\ 10^{-7}$	$1.609\ 10^{-7}$	1.129
35	$2.067\ 10^{-6}$	$2.213\ 10^{-6}$	1.071	$7.593\ 10^{-7}$	$8.302\ 10^{-7}$	1.093
40	$4.673\ 10^{-6}$	$4.776\ 10^{-6}$	1.022	$2.674\ 10^{-6}$	$2.789\ 10^{-6}$	1.043
45	$7.552\ 10^{-6}$	$7.493\ 10^{-6}$	0.992	$5.758\ 10^{-6}$	$5.781\ 10^{-6}$	1.004
50	$9.260\ 10^{-6}$	$9.109\ 10^{-6}$	0.984	$8.266\ 10^{-6}$	$8.168\ 10^{-6}$	0.988
∞	$1.049\ 10^{-5}$					
CF_2Br (λ range 170–307 nm):						
15	$5.571\ 10^{-8}$	$4.250\ 10^{-8}$	0.763	$5.091\ 10^{-9}$	$1.569\ 10^{-9}$	0.308
20	$3.538\ 10^{-7}$	$3.844\ 10^{-7}$	1.087	$1.310\ 10^{-8}$	$8.280\ 10^{-9}$	0.632
25	$1.874\ 10^{-6}$	$2.123\ 10^{-6}$	1.133	$1.287\ 10^{-7}$	$1.348\ 10^{-7}$	1.047
30	$7.700\ 10^{-6}$	$8.725\ 10^{-6}$	1.133	$1.218\ 10^{-6}$	$1.366\ 10^{-6}$	1.121
35	$2.803\ 10^{-5}$	$3.112\ 10^{-5}$	1.110	$7.864\ 10^{-6}$	$8.747\ 10^{-6}$	1.112
40	$9.850\ 10^{-5}$	$1.054\ 10^{-4}$	1.070	$4.179\ 10^{-5}$	$4.511\ 10^{-5}$	1.079
45	$2.449\ 10^{-4}$	$2.523\ 10^{-4}$	1.030	$1.482\ 10^{-4}$	$1.541\ 10^{-4}$	1.040
50	$3.735\ 10^{-4}$	$3.794\ 10^{-4}$	1.016	$3.013\ 10^{-4}$	$3.072\ 10^{-4}$	1.020
∞	$4.727\ 10^{-4}$					
CF_2BrCl (λ range 170–307 nm)						
15	$3.598\ 10^{-8}$	$4.062\ 10^{-8}$	1.129	$1.544\ 10^{-10}$	$1.013\ 10^{-10}$	0.656
20	$3.781\ 10^{-7}$	$4.372\ 10^{-7}$	1.156	$6.884\ 10^{-9}$	$7.813\ 10^{-9}$	1.135
25	$2.016\ 10^{-6}$	$2.316\ 10^{-6}$	1.149	$1.451\ 10^{-7}$	$1.662\ 10^{-7}$	1.146
30	$7.243\ 10^{-6}$	$8.243\ 10^{-6}$	1.138	$1.384\ 10^{-6}$	$1.575\ 10^{-6}$	1.138
35	$2.021\ 10^{-5}$	$2.250\ 10^{-5}$	1.113	$7.366\ 10^{-6}$	$8.225\ 10^{-6}$	1.117
40	$4.745\ 10^{-5}$	$5.102\ 10^{-5}$	1.075	$2.639\ 10^{-5}$	$2.856\ 10^{-5}$	1.082
45	$8.263\ 10^{-5}$	$8.573\ 10^{-5}$	1.038	$6.023\ 10^{-5}$	$6.296\ 10^{-5}$	1.045
50	$1.070\ 10^{-4}$	$1.094\ 10^{-4}$	1.023	$9.301\ 10^{-5}$	$9.544\ 10^{-5}$	1.026
∞	$1.263\ 10^{-4}$					

[a] Temperature independent cross-section. J_{rel} relative value $J(T)/J(295\ K)$.

mid stratosphere and gradually decreases, following the temperature profile in the stratosphere.

Due to a significant increase of the ozone optical depth in the stratosphere at wavelengths beyond 220 nm, the value of the overall photodissociation coefficients between 15 and 35 km is mainly influenced by the 200–210 nm interval contribution.

In such conditions, a significant increase of overall photodissociation coefficients is to be expected because of the strong increase of absorption cross-sections (up to 25%) at lower temperatures in this wavelength interval.

Table VII. Photodissociation coefficients versus altitude in the troposphere

Z(km)	sec $\chi = 1$			sec $\chi = 2$		
	$J(s^{-1})$ σ(295 K)[a]	$J(s^{-1})$ $\sigma = f(T)$	J_{rel}	$J(s^{-1})$ σ(295 K)[a]	$J(s^{-1})$ $\sigma = f(T)$	J_{rel}
CF_3Br (λ range 175–335 nm):						
0	$5.575\ 10^{-11}$	$4.670\ 10^{-11}$	0.838	$3.001\ 10^{-11}$	$2.498\ 10^{-11}$	0.832
2	$5.640\ 10^{-11}$	$3.272\ 10^{-11}$	0.580	$3.037\ 10^{-11}$	$1.721\ 10^{-11}$	0.567
4	$5.705\ 10^{-11}$	$1.813\ 10^{-11}$	0.318	$3.074\ 10^{-11}$	$9.192\ 10^{-12}$	0.299
6	$5.790\ 10^{-11}$	$1.267\ 10^{-11}$	0.217	$3.114\ 10^{-11}$	$6.221\ 10^{-12}$	0.200
8	$6.240\ 10^{-11}$	$1.065\ 10^{-11}$	0.171	$3.168\ 10^{-11}$	$3.185\ 10^{-12}$	0.101
10	$1.110\ 10^{-10}$	$6.012\ 10^{-11}$	0.542	$3.241\ 10^{-11}$	$1.104\ 10^{-12}$	0.034
12	$4.621\ 10^{-10}$	$4.613\ 10^{-10}$	0.998	$3.339\ 10^{-11}$	$1.148\ 10^{-12}$	0.034
14	$1.974\ 10^{-9}$	$2.193\ 10^{-9}$	1.111	$3.649\ 10^{-11}$	$3.686\ 10^{-12}$	0.101
∞	$1.049\ 10^{-5}$					
CF_2Br_2 (λ range 170–335 nm):						
0	$7.365\ 10^{-8}$	$6.450\ 10^{-8}$	0.876	$4.061\ 10^{-8}$	$3.512\ 10^{-8}$	0.865
2	$7.448\ 10^{-8}$	$5.111\ 10^{-8}$	0.686	$4.107\ 10^{-8}$	$2.719\ 10^{-8}$	0.662
4	$7.533\ 10^{-8}$	$4.064\ 10^{-8}$	0.539	$4.154\ 10^{-8}$	$2.111\ 10^{-8}$	0.508
6	$7.626\ 10^{-8}$	$3.244\ 10^{-8}$	0.425	$4.204\ 10^{-8}$	$1.645\ 10^{-8}$	0.391
8	$7.756\ 10^{-8}$	$2.613\ 10^{-8}$	0.337	$4.274\ 10^{-8}$	$1.292\ 10^{-8}$	0.302
10	$7.964\ 10^{-8}$	$2.168\ 10^{-8}$	0.272	$4.367\ 10^{-8}$	$1.024\ 10^{-8}$	0.235
12	$8.451\ 10^{-8}$	$2.347\ 10^{-8}$	0.278	$4.478\ 10^{-8}$	$9.384\ 10^{-9}$	0.210
14	$9.884\ 10^{-8}$	$3.849\ 10^{-8}$	0.389	$4.601\ 10^{-8}$	$9.718\ 10^{-9}$	0.211
∞	$4.728\ 10^{-4}$					
CF_2BrCl (λ range 170–335 nm):						
0	$4.168\ 10^{-9}$	$3.430\ 10^{-9}$	0.823	$1.680\ 10^{-9}$	$1.354\ 10^{-9}$	0.806
2	$4.238\ 10^{-9}$	$2.439\ 10^{-9}$	0.576	$1.709\ 10^{-9}$	$9.267\ 10^{-10}$	0.542
4	$4.311\ 10^{-9}$	$1.744\ 10^{-9}$	0.405	$1.740\ 10^{-9}$	$6.380\ 10^{-10}$	0.367
6	$4.389\ 10^{-9}$	$1.255\ 10^{-9}$	0.286	$1.773\ 10^{-9}$	$4.419\ 10^{-10}$	0.249
8	$4.534\ 10^{-9}$	$9.546\ 10^{-10}$	0.211	$1.819\ 10^{-9}$	$3.100\ 10^{-10}$	0.170
10	$5.139\ 10^{-9}$	$1.243\ 10^{-9}$	0.242	$1.881\ 10^{-9}$	$2.207\ 10^{-10}$	0.117
12	$8.702\ 10^{-9}$	$5.112\ 10^{-8}$	0.587	$1.957\ 10^{-9}$	$1.957\ 10^{-10}$	0.100
14	$2.352\ 10^{-8}$	$2.213\ 10^{-8}$	0.941	$2.061\ 10^{-9}$	$2.303\ 10^{-10}$	0.112
∞	$1.263\ 10^{-4}$					

[a] Temperature independent cross-section. J_{rel} relative value $J(T)/J(295\ K)$.

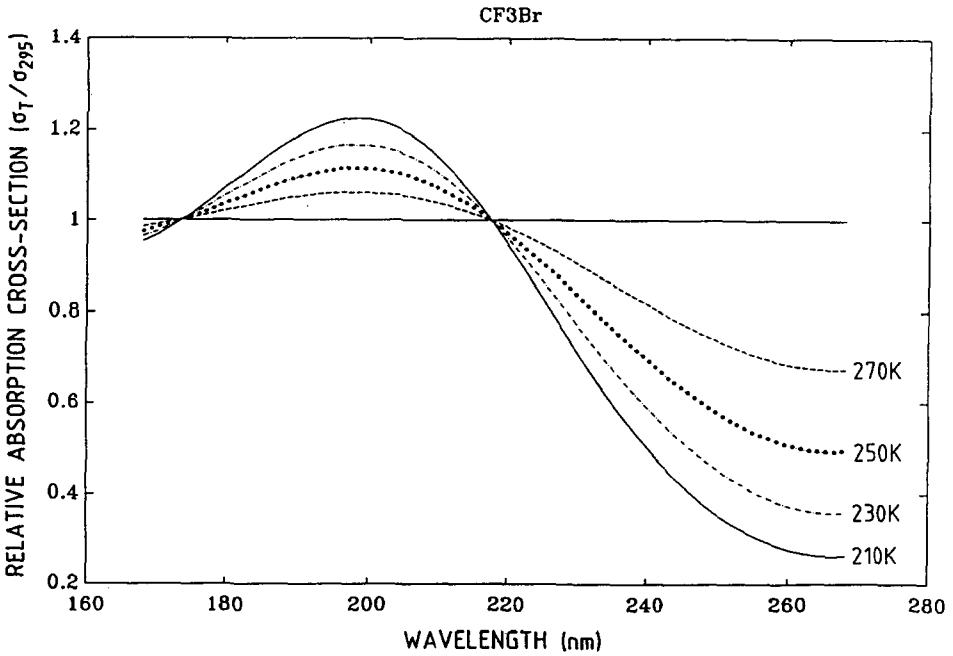

Fig. 10. Relative absorption cross-sections $\sigma(T)/\sigma(295\ \text{K})$ of CF_3Br as a function of wavelength ($T = 270$ K, 250 K, 230 K and 210 K).

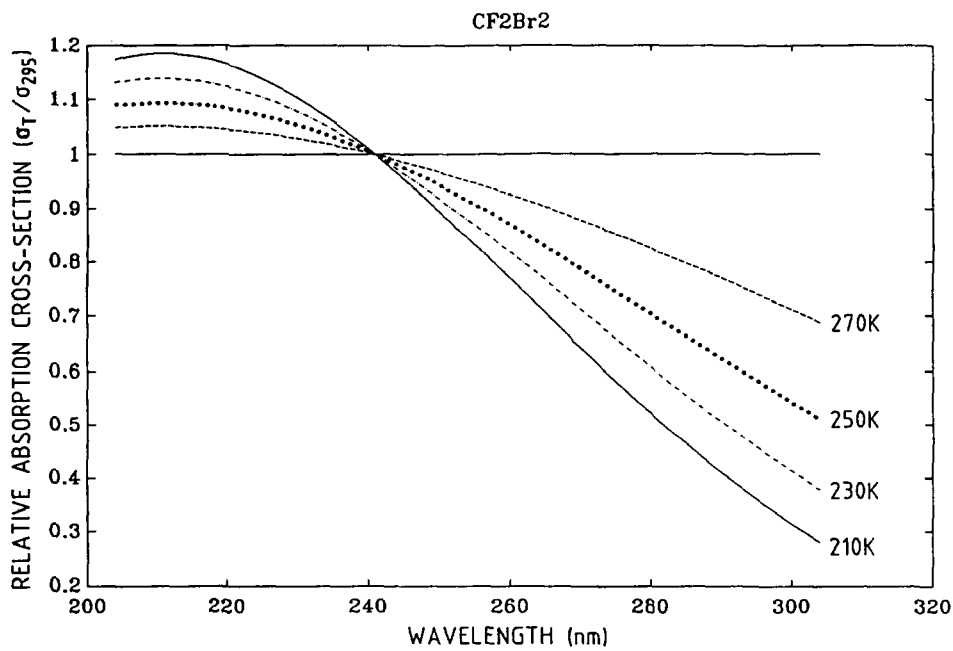

Fig. 11. Relative absorption cross-sections $\sigma(T)/\sigma(295\ \text{K})$ of CF_2Br_2 as a function of wavelength ($T = 270$ K, 250 K, 230 K and 210 K).

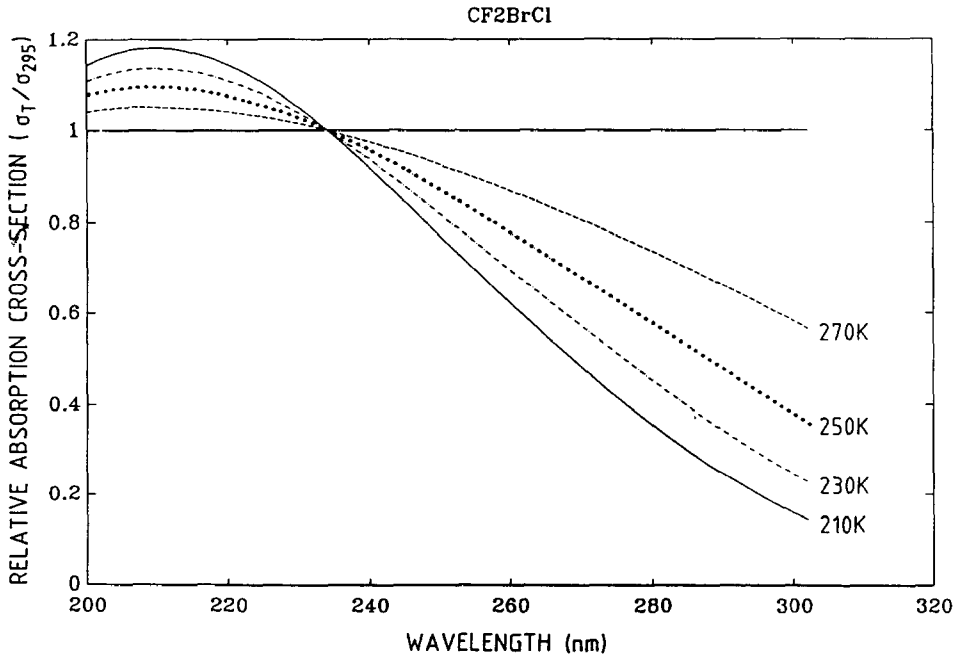

Fig. 12. Relative absorption cross-sections $\sigma(T)/\sigma(295\ \text{K})$ of CF_2Br_2 as a function of wavelength ($T = 270$ K, 250 K, 230 K and 210 K).

The introduction of higher photodissociation coefficients in atmospheric models decreases altitudes of photolysis and, therefore, changes the altitude profile of the considered halomethane in the stratosphere.

Calculations have also been made for the troposphere, between 0 to 14 km altitudes. To perform these calculations, the values of the absorption cross-sections have been extrapolated, taking into account an exponential decrease of absorption cross-sections with respect to the wavelength.

The results, presented in Table VII, are in good agreement with the integrated values of the photodissociation coefficients over all the tropospheric range proposed by Molina *et al.* (1982).

In conclusion, this work presents a complete and coherent set of experimental data showing a nonnegligible temperature dependence of the absorption cross-sections and photodissociation coefficients of bromo-fluoro-methanes. It gives fairly simple parametrical functions to compute the absorption cross-section values with respect of temperature and wavelength.

Acknowledgements

The authors wish to thank Dr G. Brasseur for helpful discussions, Mr L. Dierickx who performed some of the measurements and Mr E. Falise who performed the computer calculations of the photodissociation coefficients.

References

Berg, W. W., Heidt, L. E., Pollock, W., Sperry, P. D., Cicerone, R. J., and Gladney, E. S., 1984, Brominated organic species in the Arctic atmosphere, *Geophys. Res. Lett.* **11**, 429–432.

Brasseur, G. and Simon, P. C., 1981, Stratospheric and thermal response to long-term variability in solar UV irradiance, *J. Geophys. Res.* **86**, 7343–7362.

Brasseur, G. and Simon, P. C., 1988, Changes in stratospheric ozone: observations and theories, *Aeronomica Acta* **A334**.

Class, Th., Kohnle, R., Ballschmiter, K., 1986, Chemistry of organic races in air VII: Bromo- and bromochloromethanes in air over Atlantic Ocea, *Chemosphere* **15**, 429–436.

Cicerone, R. J., Heidt, L. E., and Pollock, W. H., 1988, Measurements of atmospheric methyl bromide (CH_3Br) and bromoform ($CHBr_3$), *J. Geophys. Res.* **93**, 3745–3749.

Fabian, P., Borchers, R., Penkett, S. A., and Prosser, N. J. D., 1981, Halocarbons in the stratosphere, *Nature* **294**, 733–735.

Gillotay, D. and Simon, P. C., 1988, Ultraviolet absorption cross-sections of methyl bromide at stratospheric temperatures, *Ann. Geophysicae* **6**, 211–215.

Kockarts, G., 1976, Absorption and photodissociation in the Schumann–Runge bands of molecular oxygen in the terrestrial atmosphere, *Planet. Space Sci.* **24**, 589–604.

Lal, S., Borchers, R., Fabian, P., and Kruger, B. C., 1985, Increasing abundance of $CBrClF_2$ in the atmosphere, *Nature* **316**, 135–136.

Molina, L. T., Molina, M. J., and Rowland, F. S., 1982, Ultraviolet absorption cross-sections of several brominated methanes and ethanes of atmospheric interest, *J. Phys. Chem.* **86**, 2672–2676.

Nicolet, M., 1984, On the molecular scattering in the terrestrial atmosphere: an empirical formula for calculation in the homosphere, *Planet. Space Sci.* **32**, 1467–1468.

Penkett, S. A., Jones, B. M. R., Rycroft, M. J., and Simmons, D. A., 1985, An interhemispheric comparison of the concentrations of bromide compounds in the atmosphere, *Nature* **318**, 550–553.

Prather, M. J., McElroy, M. B., and Wofsy, S. C., 1984, Reductions in ozone at high concentrations of stratospheric halogens, *Nature* **312**, 227–231.

Rodriguez, J. M., Ko, M. K. M., and Sze, N. D., 1986, Chlorine chemistry in the Antarctic stratosphere: Impact of OClO and Cl_2O_2 and implications for observations, *Geophys. Res. Lett.* **13**, 1292–1295.

Simon, P. C., Gillotay, D., Vanlaethem-Meuree, N., and Wisemberg, J., 1988, Ultraviolet absorption cross-sections of chloro- and chlorofluoro-methanes at stratospheric temperatures, *J. Atmos. Chem.* **7**, 107–135.

WMO, 1985, *Atmospheric Ozone 1985*, WMO global ozone research and monitoring project, Report 16, vol. I, pp. 355–367.

Yung, Y. L., Pinto, J. P., Watson, R. T., and Sander, S. P., 1980, Atmospheric bromine and ozone perturbations in the lower stratosphere, *J. Atmos. Sci.* **37**, 339–353.